Cell Free Expression and Functional Reconstitution of Eukaryotic Drug Transporters[†]

Thorsten Keller,[‡] Daniel Schwarz,[§] Frank Bernhard,[§] Volker Dötsch,[§] Carola Hunte,[||] Valentin Gorboulev,[‡] and Hermann Koepsell[‡,*]

Institute of Anatomy and Cell Biology, University of Würzburg, Koellikerstrasse 6, 97070 Würzburg, Germany, Department of Biophysical Chemistry, University of Frankfurt, Frankfurt, Germany, and Department of Molecular Membrane Biology, Max Planck Institute of Biophysics, Frankfurt, Germany

Received January 11, 2008; Revised Manuscript Received February 26, 2008

ABSTRACT: Polyspecific organic cation and anion transporters of the *SLC22* protein family are critically involved in absorption and excretion of drugs. To elucidate transport mechanisms, functional and biophysical characterization of purified transporters is required and tertiary structures must be determined. Here, we synthesized rat organic cation transporters OCT1 and OCT2 and rat organic anion transporter OAT1 in a cell free system in the absence of detergent. We solubilized the precipitates with 2% 1-myristoyl-2-hydroxy-*sn*-glycero-3-[phospho-*rac*-(1-glycerol)] (LMPG), purified the transporters in the presence of 1% 3-[(3-cholamidopropyl)dimethylammonio]-1-propanesulfonate (CHAPS) or octyl glucoside, and reconstituted them into proteoliposomes. From 1 mL reaction vessels 0.13–0.36 mg of transporter proteins was purified. Thus, from five to ten 1 mL reaction vessels sufficient protein for crystallization was obtained. In the presence of 1% LMPG and 0.5% CHAPS, OCT1 and OAT1 formed homo-oligomers but no hetero-oligomers. After reconstitution of OCT1, OCT2, and OAT1 into proteoliposomes, similar Michaelis−Menten K_m values were measured for uptake of 1-methyl-4-phenylpyridinium and *p*-aminohippurate (PAH^-) by the organic cation and anion transporters, respectively, as after expression of the transporters in cells. Using the reconstituted system, evidence was obtained that OAT1 operates as obligatory and electroneutral PAH^-/dicarboxylate antiporter and contains a low-affinity chloride binding site that stimulates turnover. PAH^- uptake was observed only with α-ketoglutarate (KG^{2-}) on the *trans* side, and *trans*-KG^{2-} increased the PAH^- concentration in voltage-clamped proteoliposomes transiently above equilibrium. The V_{max} of PAH^-/KG^{2-} antiport was increased by Cl^- in a manner independent of gradients, and PAH^-/KG^{2-} antiport was independent of membrane potential in the absence or presence of Cl^-.

Polyspecific transporters of the *SLC22* transporter family play a pivotal role in the elimination and distribution of drugs, toxins, and endogenous compounds such as carnitine, choline, acetylcholine, and monoamine neurotransmitters (*1–3*). The family contains organic cation transporters (OCTs),[1] organic anion antiporters (OATs), and Na^+-carnitine cotransporters (OCTNs). The biomedical importance of these transporters is hallmarked by the findings that (a) primary systemic carnitine deficiency is caused by defect mutations of the carnitine transporter OCTN2 (*4, 5*), (b) several autoimmune diseases are associated with mutations in transporters OCTN1 and OCTN2 (*6–8*), (c) OCT1 is critically involved in uptake of the antidiabetic drug metformin into liver and patients with loss-of function mutations in OCT1 do not respond to metformin treatment (*9*), and (d) OCT1 mediates uptake of the cytostatic drug imantinib into chronic myeloid leukemia cells and treatment with imantinib becomes ineffective when expression of OCT1 is down-regulated during therapy (*10*).

Cloning, localization, and functional characterization of recombinant transporters provided new insights into the function of polyspecific transporters of the *SLC22* family (*11–17*). With the exception of electrical measurements performed in giant patches of *Xenopus laevis* oocytes expressing the highly active electrogenic organic cation transporter 2 from rat (rOct2, *Slc22a2*) (*12*), possibilities for functional characterization were restricted because the compositions of ions and substrates could not be controlled on both sides of the plasma membrane.

After the crystal structures of lactose permease and the glycerol 3-phosphate transporter from *Escherichia coli* that belong to the same superfamily as the OCTs had been

[†] This work was supported by the Deutsche Forschungsgemeinschaft (Grant SFB 487/A4 to V.G. and H.K. and Grant EXC 115 to C.H.).

* To whom correspondence should be addressed. Phone: ++49-(0)931 312700. Fax: ++49-(0)931 312087. E-mail: Hermann@Koepsell.de.

[‡] University of Würzburg.

[§] University of Frankfurt.

[||] Max Planck Institute of Biophysics.

[1] Abbreviations: OCT, organic cation transporter; OAT, organic anion transporter; OCTN, Na^+-carnitine cotransporter; CF, cell free; PAH^-, *p*-aminohippuric acid; KG^{2-}, α-ketoglutaric acid; MPP^+, 1-methyl-4-phenylpyridinium; CHAPS, 3-[(3-cholamidopropyl)dimethylammonio]-1-propanesulfonate; LMPG, 1-myristoyl-2-hydroxy-*sn*-glycero-3-[phospho-*rac*-(1-glycerol)]; Ni^{2+}-NTA-agarose, nickel(II)-charged nitrilotriacetic acid agarose; CD, circular dichroism; TEA^+, tetraethylammonium; $TBuA^+$, tetrabutylammonium; $TPeA^+$, tetrapentylammonium; HRP, horseradish peroxidase; TMH, transmembrane α-helix; GPCR, G-protein-coupled receptor; aa, amino acid(s); HEK, human embryonic kidney.

10.1021/bi800060w CCC: $40.75
Published on Web 03/25/2008

determined (*18*), structural models of OCTs and OATs could be constructed that were employed to interpret mutagenesis experiments (*19, 20*). Several features of these models could be confirmed by mutagenesis (*19–22*); however, they did not provide detailed molecular information that allowed elucidation of transport mechanisms. Therefore, the tertiary structure must be known. Recently, we succeeded in expressing the rat organic cation transporter rOct1 (*Slc22a1*) in insect cells, purifiying the transporter, and reconstituting transport activity in proteoliposomes (*23*). However, from insect cells only small amounts of purified protein were obtained that did not allow us to start crystallization attempts.

This paper describes cell free (CF) expression and functional reconstitution of the rat organic cation transporters rOct1 and rOct2 and of the rat organic anion transporter rOat1 (*Slc22a6*). By CF expression, milligram amounts of purified transporters can be obtained within 3 days. Functional characterization of purified and reconstituted rOat1 provided evidence that rOat1 is an obligate electroneutral *p*-aminohippurate (PAH^-)/α-ketoglutarate (KG^{2-}) exchanger which is modulated by a low-affinity chloride binding site.

MATERIALS AND METHODS

Materials. [^{3}H]-1-Methyl-4-phenylpyridinium (MPP^+) (3.1 TBq/mmol) and [^{14}C]-*p*-aminohippuriate (PAH^-) (2.0 GBq/mmol) were obtained from Biotrend (Köln, Germany). Agarose coupled with anti-FLAG antibody, anti-FLAG antibody from mice, horseradish peroxidase−anti-mouse IgG conjugate, and FLAG peptide were purchased from Sigma-Aldrich (Taufkirchen, Germany). 3-[(3-Cholamidopropyl)dimethylammonio]-1-propanesulfonate (CHAPS) was obtained from AppliChem (Darmstadt, Germany) and 1-myristoyl-2-hydroxy-*sn*-glycero-3-[phospho-*rac*-(1-glycerol)] (LMPG) from Avanti Polar Lipids (Alabaster, AL). All other chemicals were obtained as described previously (*23*).

DNA Constructs of Tagged Transporters. Constructs for CF expression of transporters were cloned into vector pET21a (Novagen, Darmstadt, Germany). *Bam*HI and *Xho*I restriction sites were used retaining an open reading frame with an NH_2-terminal T7 tag.

(i) Cloning of Plasmids (T7)rOct1(His)/pET21a and (T7)-rOct2(His)/pET21a. Polymerase chain reactions (PCRs) were performed with forward primers corresponding to the NH_2 terminus of rOct1 (*11*) or rOct2 (*24*) and reverse primers corresponding to the COOH termini of the respective transporters. The forward and reverse primers contained *Bam*HI and *Xho*I sites, respectively. PCR amplificates covering the complete open reading frame of rOct1 and rOct2 were cut with *Bam*HI and *Xho*I, gel-purified, and ligated into vector pET21a.

(ii) Cloning of Plasmid (T7)rOct1(FLAG)/pET21a. In plasmid rOct1(His)/pET21a, the *Eco*RI/*Xho*I fragment comprising the His-tagged COOH-terminal part of rOct1 was replaced with the respective FLAG-tagged *Eco*RI/*Xho*I fragment obtained from FLAG-tagged rOct1 in vector pRSSP (*19*).

(iii) Cloning of Plasmid (T7)rOat1(FLAG)/pET21a. On the basis of the pSRORT1 plasmid that contained rOat1 (*25, 26*) with COOH-terminal FLAG tag kindly provided by N. A. Wolff (Witten/Herdecke, Germany), a PCR amplificate comprising the complete open reading frame of FLAG-tagged rOat1 was prepared using forward and reverse primers with *Bam*HI and *Xho*I sites, respectively. After digestion with *Bam*HI and *Xho*I, the amplificate was gel-purified and ligated into plasmid pET21a.

(iv) Cloning of Plasmid (T7)rOat1(His)/pET21a. The 3′-part of rOat1 was PCR-amplified from rat kidney using a forward primer corresponding to nucleotides 871–888 (numbering from GenBank accession number AB004559) and a reverse primer that covered the last COOH-terminal amino acids of rOat1 and contained a *Xho*I site. The PCR product was cut with *Xma*I and *Xho*I, and the obtained 260 bp fragment was isolated and substituted for the respective fragment encoding rOat1(FLAG) in the (T7)rOat1(FLAG)/pET21a plasmid. All constructs were sequenced to rule out PCR errors.

Cell Free Expression of Transport Proteins. Bacterial CF extracts were prepared from *E. coli* strain A19 (*E. coli* Genetic Stock Center, New Haven, CT) and frozen in liquid nitrogen (*27*). CF expression was performed in the continuous exchange mode using a membrane with a cutoff of 25 kDa to separate the reaction mixture with ribosomes and enzymes from the feeding mixture. The reaction mixture and feeding mixture were created as described previously (*27*). Dispodialysers (1 mL reaction volume) from Spectrum Laboratories Inc. (Breda, The Netherlands) in glass tubes containing 15 mL of feeding mixture were used. Incubation for protein synthesis was performed for 20 h at 30 °C on a shaker. Precipitated proteins were spun down by 10 min centrifugation at 10000*g* (4 °C). For affinity purification on Ni^{2+}-NTA-agarose, pellets were washed with Tris buffer [20 mM Tris-HCl (pH 8) and 500 mM NaCl] containing 10 mM imidazole. For immunoaffinity purification using anti-FLAG antibody coupled to agarose, washing was performed with Hepes buffer [20 mM Hepes-NaOH (pH 7.5) and 150 mM NaCl]. The washed precipitates were solubilized by incubation for 1 h at 30 °C with 1 mL of 2% (w/v) 1-myristoyl-2-hydroxy-*sn*-glycero-3-[phospho-*rac*-(1-glycerol)] (LMPG) dissolved in Tris buffer containing 10 mM imidazole (His-tagged transporters) or in Hepes buffer (FLAG-tagged transporters). The suspensions were centrifuged for 10 min at 10000*g* (4 °C), and the supernatants (LMPG supernatants) were used for purification.

Affinity Purification of Transporters. For affinity purification on Ni^{2+}-NTA-agarose, to 1 mL of LMPG supernatant were added (a) 10 mL of Tris buffer containing 10 mM imidazole and 1% (w/v) CHAPS and (b) 1 mL of Ni^{2+}-NTA-agarose that was equilibrated with the respective detergent in Tris buffer containing 10 mM imidazole. After incubation for 1 h at 4 °C, the suspension was poured into a column and washed with 10 mL of Tris buffer containing 1% CHAPS and 10 mM imidazole. After additional washing with Tris buffer (10 mL) containing 1% CHAPS and 20 mM imidazole, proteins were eluted with 5 mL of Tris buffer containing 1% CHAPS and 100 mM imidazole. During elution, 250 μL fractions were collected.

For immunoaffinity purification, 0.5 mL of agarose beads coupled to an anti-FLAG antibody that had been equilibrated with Hepes buffer containing 1% CHAPS (Hepes-CHAPS) or 1% ocytyl glucoside (Hepes-OG) was mixed with 10 mL of Hepes-CHAPS or Hepes-OG, respectively, and 1 mL of LMPG supernatant was added. The suspension was incubated overnight at 4 °C. The beads were separated via centrifuga-

tion for 10 min at 500*g* and washed with Hepes-CHAPS or Hepes-OG, and transport proteins were eluted by overnight incubation at 4 °C with 1 mL of Hepes-CHAPS or Hepes-OG containing 0.2 mg/mL antigenic FLAG peptide. Beads were removed via centrifugation for 10 min at 500*g*.

Gel Filtration of Purified Transporters. For each analysis, purified rOat1 protein dissolved in 50 μL of Hepes-CHAPS or Hepes-OG was applied to a Superdex 200 PC 3.2/30 column in a SMART system (GE Healthcare, München, Germany). The column was equilibrated with Hepes-CHAPS or Hepes-OG, and gel filtration was performed with a flow rate of 50 μL/min. It was calibrated using aldolase (158 kDa), bovine serum albumin (67 kDa), and ribonuclease A (13.7 kDa) supplied by GE Healthcare.

Coprecipitation of His-Tagged and FLAG-Tagged Transporters. To investigate interactions between rOct1, rOct2, and/or rOat1, LMPG supernatant (100 μL with 20 μg of protein) containing one in vitro-expressed transporter with a His tag was mixed with LMPG supernatant (100 μL with 20 μg of protein) containing an in vitro-expressed FLAG-tagged transporter and diluted with 200 μL of Tris buffer containing 1% CHAPS and 10 mM imidazole (final detergent concentrations, 1% LMPG and 0.5% CHAPS) and incubated for 1 h at 4 °C; 100 μL of Ni^{2+}-NTA-agarose equilibrated with Tris buffer containing 1% LMPG, 0.5% CHAPS, and 10 mM imidazole was added and the suspension incubated for an additional 1 h at 4 °C, and the beads were separated via centrifugation for 10 min at 500*g* (room temperature). The beads were washed five times at room temperature with 1 mL of Tris buffer containing 1% CHAPS and 10 mM imidazole-CHAPS and five times with Tris buffer containing 1% CHAPS and 20 mM imidazole. For protein elution, pelleted beads were suspended for 10 min at room temperature in 400 μL of Tris buffer containing 1% CHAPS and 100 mM imidazole, and the suspension was centrifuged for 10 min at 500*g*. The supernatants were collected, and FLAG-tagged transporters were analyzed by Western blots.

Circular Dichroism Spectroscopy. Circular dichroism (CD) spectroscopy of purified FLAG-tagged rOat1 was performed with a Jasco J-810 spectropolarimeter (Jasco Labortechnik, Gross-Umstadt, Germany). The monomeric fraction of rOAT1 obtained after gel filtration was dialyzed against a 10 mM sodium phosphate buffer (pH 8.0) containing 1% octyl glucoside. Assays were carried out at standard sensitivity with a bandwidth of 3 nm and a response of 1 s. The data pitch was 0.2 nm and the scanning rate 50 nm/min. The α-helical content of rOAT1 was calculated as described by Rohl and Baldwin (*28*). The theoretical α-helical content according to primary structure was calculated with the PREDICT PROTEIN server at http://cubic.bioc.columbia.edu/pp (*29*).

Reconstitution of Purified Transporters by a Detergent-Removal Freeze–Thaw Procedure. Reconstitution into proteoliposomes was performed in three steps as described previously (*23, 30*). First, small proteoliposomes and protein–lipid aggregates were formed by detergent removal. Second, large multilamellar liposomes were added, and the mixture was frozen and thawed. Third, transporting large proteoliposomes were generated by mixing the small proteoliposomes and protein–lipid aggregates with the large multilamellar liposomes, freezing and thawing, pelleting, and homogenizing. For formation of small proteoliposomes and protein–lipid aggregates, cholesterol (1 mg), phosphatidylcholine (1 mg), and phosphatidylserine (1 mg) were dissolved in 1 mL of a chloroform/methanol mixture (1/1, v/v) and dried in a round-bottom flask under a stream of nitrogen, and 500 μL of purified transporter proteins was added. The added transporter proteins were solubilized in (a) Tris buffer containing 1% CHAPS and 100 mM imidazole, (b) Tris buffer containing 1% octyl glucoside and 100 mM imidazole, or (c) Hepes buffer containing 1% CHAPS and antigenic peptides. The round-bottom flasks were shaken for 1 h at 4 °C, and the respective detergent and the antigenic peptide used for immunoaffinity purification were removed by dialysis at 4 °C against 20 mM Tris-HCl (pH 7.9), 500 mM NaCl, and 100 mM choline chloride. The obtained suspensions of small proteoliposomes and protein–lipid aggregates were centrifuged for 30 min at 200000*g* (4 °C). The sediments were resuspended in 2 mL of ice-cold vesicle loading buffers that contained 20 mM imidazole (pH 7.4), 0.1 mM Mg^{2+}, and various concentrations of cyclamate$^-$, Cl^-, α-ketoglutarate (KG^{2-}), K^+, and/or Na^+. After another 30 min centrifugation at 200000*g*, the sediments were suspended in 150 μL of the respective loading buffer and stored at 4 °C. To prepare large multilamellar liposomes, 4 mg of phosphatidylserine and 2 mg of cholesterol were dissolved in 1 mL of a chloroform/methanol mixture (1/1, v/v) and dried in a round-bottom flask under a stream of nitrogen. One milliliter of loading buffer was added, and the flask was shaken for 3 h at room temperature under nitrogen. Large aggregates were pelleted via centrifugation for 10 min at 10000*g* (room temperature), and multilamellar liposomes in the supernatant were concentrated by centrifugation at 200000*g* for 15 min and resuspension of the pellet in 150 μL of loading buffer (room temperature). To form transporting large proteoliposomes, 150 μL of the protein–lipid aggregates was mixed with 150 μL of the multilamellar liposomes and incubated for 15 min at 41 °C. This mixture was snap-frozen in liquid nitrogen. Shortly before transport measurements were started, the sample was thawed via incubation for 5 min at 37 °C in a water bath. After addition of 1.7 mL of loading buffer (room temperature), the proteoliposomes were spun down by centrifugation at 200000*g* for 15 min (room temperature). The pellet was suspended in 300 μL of loading buffer (room temperature), and formation of monolamellar proteoliposomes was induced by repeated suction of the suspension into and forced extrusion out of a 100 μL pipet tip.

Uptake Measurements in Proteoliposomes. For measurements of the rates of MPP^+ or PAH^- uptake, proteoliposomes filled with various loading buffers were preincubated for 10 min at 37 °C in the absence or presence of 20 μM valinomycin. For measurements of MPP^+ uptake, the preincubation was performed without or with 100 μM quinine, an inhibitor of rOct1 and rOct2 (*3*). Uptake of MPP^+ was performed in the absence of quinine using proteoliposomes that were preincubated without quinine, or in the presence 100 μM quinine using the quinine preincubated proteoliposomes. Uptake of PAH^- was performed in the absence or presence of 2 mM probenecid, an inhibitor of rOat1 (*25, 26*). Uptake was initiated by mixing 10 μL of prewarmed proteoliposomes (37 °C) with 90 μL (rOct1 or rOct2) or 490 μL (rOat1) of prewarmed (37 °C) transport medium consist-

ing of 20 mM imidazole (pH 7.4), 0.1 mM Mg^{2+}, and various concentrations of cyclamate$^-$, Cl^-, Na^+, K^+, and/or 0.5 mM α-ketoglutarate. For MPP^+ uptake measurements, the transport medium contained 12 nM [^{3}H]MPP^+ without or with nonradioactive MPP^+, tetraethylammonium (TEA^+), tetrabutylammomium ($TBuA^+$), or tetrapentylammomium ($TPeA^+$). For PAH^- uptake measurements, the transport medium contained 5 μM [^{14}C]PAH^- without or with nonradioactive PAH^-. After incubation for 1 s or longer time periods, uptake was stopped by adding 1 mL of ice-cold stop solution [for MPP^+ uptake, 20 mM imidazole (pH 7.4), 0.1 mM magnesium cyclamate, and 100 mM potassium cyclamate (KC buffer) containing 100 μM quinine; for PAH^- uptake, KC buffer containing 2 mM probenecid].

For measurement of the radioactivity within proteoliposomes, the proteoliposomes suspended in stop solution were applied to 0.22 μm cellulose acetate filters (Millipore GSWP) and washed with 10 mL of the respective ice-cold stop solution. The filters were dissolved in LUMASAFE PLUS cocktail (Lumac LSC, Groningen, The Netherlands) and assayed for radioactivity.

SDS−Polyacrylamide Gel Electrophoresis (SDS−PAGE) and Western Blotting. For SDS−PAGE, protein samples were pretreated for 30 min at 37 °C in 60 mM Tris-HCl (pH 6.8), 100 mM dithiothreitol, 2% (w/v) SDS, and 7% (v/v) glycerol and then separated by SDS−PAGE as described previously (*31*). Separated proteins were transferred by electroblotting to a polyvinylidene difluoride membrane. For immunostaining of transporters, either an antibody against the T7 tag coupled to horseradish peroxidase (HRP) diluted 1/10000 (Novagen) or an anti-FLAG antibody raised in mice diluted 1/20000 (Sigma-Aldrich) and successively anti-mouse IgG coupled to HRP diluted 1/5000 (Sigma-Aldrich) were used. Binding of HRP-coupled antibodies was visualized using enhanced chemiluminescence (ECL system; Amersham Buchler, Braunschweig, Germany). Prestained molecular weight markers (BenchMark; Life Technologies, Karlsruhe, Germany) were used to determine apparent molecular masses.

Quantification and Statistics. Staining of proteins in Western blots was quantified by densitometry as described previously (*32*). GraphPad Prism version 4.1 (GraphPad Software, San Diego, CA) was used to compute statistical parameters. Apparent K_m values ± the standard error (SE) of individual experiments were determined by fitting the Michaelis−Menten equation to the data. For inhibition of tracer cation uptake by nonlabeled cations, $IC_{0.5}$ values ± SE of individual experiments were calculated by fitting the Hill equation to the data. Mean K_m, V_{max}, and $IC_{0.5}$ values ± the standard deviation (SD) of independent experiments are presented. An unpaired, two-sided Student's *t* test was used to prove statistical significance of differences between two groups. For comparison of three or more groups, an ANOVA test with post hoc Tukey comparison was employed. In the figures, typical experiments are presented.

RESULTS

Cell Free Expression and Purification of Oct1, Oct2, and Oat1 from Rat. rOct1, rOct2, and rOat1 containing NH_2-terminal T7 tags and either a COOH-terminal His tag or a COOH-terminal FLAG tag were expressed in vitro using *E. coli* extracts. The produced transporters precipitated in the detergent free reaction buffer. The precipitates were spun down at 10000*g*, washed, and solubilized with 2% LMPG. After removal of aggregates, transporters were purified in the presence of 1% CHAPS or 1% octyl glucoside. His-tagged transporters were affinity-purified on Ni^{2+}-NTA-agarose beads, whereas FLAG-tagged transporters were immunopurified on anti-FLAG antibodies coupled to agarose beads using antigenic peptide for elution. In Coomassie- and silver-stained SDS−polyacrylamide gels, single protein bands with apparent molecular masses of ∼55 kDa (rOct1 and rOct2) or ∼60 kDa (rOat1) were obtained (Figure 1). The transporters were identified in Western blots with antibodies against the T7 or FLAG tag. From 1 mL of transcription/translation mixture, 120 ± 17 μg of rOct1 ($n = 3$), 138 ± 18 μg of rOct2 ($n = 3$), and 134 ± 13 μg of rOat1 ($n = 3$) were purified in the presence of CHAPS using Ni^{2+}-NTA-agarose. The efficiency of CF expression of FLAG-tagged rOct1 and rOat1 was higher compared to that of the His-tagged transporters. From 1 mL of in vitro transcription/translation mixture, 240 μg of rOct1 protein (one experiment) and 359 ± 38 μg of rOat1 protein ($n = 3$) were obtained after purification in the presence of CHAPS. After purification in the presence of octyl glucoside, 337 ± 19 μg of rOat1 protein ($n = 3$) was isolated.

To investigate purified FLAG-tagged rOat1 protein for homogeneity, we subjected rOat1 purified in presence of 1% CHAPS or 1% octyl glucoside to size exclusion gel chromatography on an analytical Superdex 200 column in the presence of 1% CHAPS or 1% octyl glucoside, repectively (Figure 2A,B). Symmetric main elution peaks with apparent molecular masses similar to that of bovine serum albumin (68 kDa) were obtained, suggesting that most transporter molecules were present as monomers with some bound detergent. In addition, side peaks corresponding to 2−3-fold higher molecular masses were observed. SDS−PAGE indicated that all peaks consisted exclusively of rOat1. The data show that a fraction of the transporter forms aggregates or homo-oligomers in the presence of 1% CHAPS or 1% octyl glucoside, yet the monomer fraction in the presence of octyl glucoside appeared to be stable. When the sample was rechromatographed in the presence of 1% octyl glucoside directly after the first chromatography, no high-molecular weight peak was observed (Figure 2C). The secondary structure of the rechromatographed monomeric peak rOat1 was analyzed by CD spectroscopy at 25 °C in the presence of 1% octyl glucoside (Figure 3). The spectrum showed minima at 208 and 222 nm and a large peak of positive ellipticity centered at 193 nm, representing characteristic features of an α-helical protein. The analysis of the spectra yielded an estimate of 54% α-helical content. The theoretical α-helical content predicted from the primary structure was 57% (*29*). The data suggest that purified FLAG-tagged rOat1 monomers are folded properly in the presence of 1% octyl glucoside.

Interaction of Separately Synthesized Transporters. We tested whether transporters form homo- and heteromers in the presence of detergent. His-tagged rOat1 and FLAG-tagged rOat1 were synthesized separately and solubilized with 2% LMPG. After removal of large aggregates, the two LMPG supernatants were mixed, diluted with an equal volume of buffer containing 1% CHAPS, and incubated for

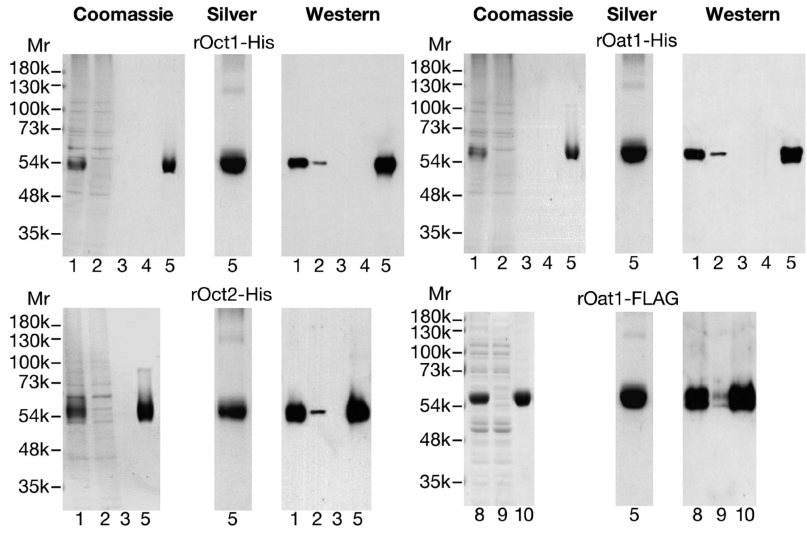

FIGURE 1: In vitro expression and purification of rOct1, rOct2, and rOat1. rOct1, rOct2, and rOat1 with C-terminal His tags (rOct1-His, rOct2-His, and rOat1-His, respectively) and rOat1 with a C-terminal FLAG tag (rOat-FLAG) were expressed in vitro using a reaction volume of 1 mL. The precipitated transport proteins were pelleted, washed, and solubilized in 1 mL of 2% LMPG. The supernatants obtained after centrifugation for 10 min at 10000*g* (LMPG supernatants) are shown in lanes 1 and 8. For Ni^{2+} affinity purification (top two panels and bottom left panel), the LMPG supernatants of the His-tagged transporters were diluted with 10 mL of Tris buffer containing 1% CHAPS and 10 mM imidazole (lane 1) and incubated with Ni^{2+}-NTA-agarose beads. The beads were poured into columns and the effluents collected (lane 2). The columns were washed with 10 mL of Tris buffer containing 1% CHAPS with either 10 mM imidazole (lane 3) or 20 mM imidazole (lane 4). Finally, the transporters were eluted with 5 mL of Tris buffer containing 1% CHAPS with 100 mM imidazole, and six 250 μL elution fractions containing the purified transporters were combined (lane 5). For immunoaffinity purification of FLAG-tagged rOat1 (bottom right panel), the LMPG supernatant was diluted with 10 mL of Hepes-CHAPS buffer (lane 8), 500 μL of agarose beads coupled to anti-FLAG antibody was added, and the suspension was incubated overnight. After centrifugation, the supernatant was analyzed (lane 9). The beads were washed, and rOat1 was eluted by incubating the beads in 1 mL of Hepes-CHAPS containing antigenic FLAG peptide. After centrifugation, the supernatant was analyzed (lane 10). The SDS−polyacrylamide gels were stained with Coomassie brilliant blue or silver. For Coomassie and silver staining of gels, 7.5 μL was applied per lane, whereas for Western blotting, 1 μL was applied per lane. Western blots with rOct1, rOct2, and His-tagged rOat1 were stained with a HRP conjugate with an antibody against the T7 tag. The Western blot with FLAG-tagged rOat1 was stained with mouse anti-FLAG antibody and the HRP conjugate with anti-mouse IgG. The figure indicates in vitro expression and purification of rOct1, rOct2, and rOat1.

1 h at 4 °C. Thereafter, Ni^{2+}-NTA-agarose beads were added, and the mixture was incubated for an additional 1 h at 4 °C. After the beads had been pelleted, less than 2% of FLAG-tagged rOat1 (one experiment) was detected in the supernatant (Figure 4, top right panel, lane 2). After extensive washing, His-tagged rOat1 was detached from the Ni^{2+}-NTA-agarose beads by incubation with 100 mM imidazole and 1% CHAPS. Together with His-tagged rOat1, at least 98% of FLAG-tagged rOat1 was detached from the beads. The data indicate that FLAG-tagged rOat1 associates nearly quantitatively with His-tagged rOat1 in the presence of 1% LMPG and 0.5% CHAPS.[2] A very similar result was obtained with rOct1 (Figure 4, top left panel). When solubilized FLAG-tagged rOct1 was mixed with solubilized His-tagged rOct1 and incubated with Ni^{2+}-NTA-agarose beads, 4.7 ± 2.1% of FLAG-tagged rOct1 remained in the supernatant and 93 ± 2.1% of FLAG-tagged rOct1 could be eluted from washed beads ($n = 3$). To evaluate whether the observed association of separately synthesized transporters represents specific oligomerization versus nonspecific protein association, we also investigated association between rOct1 and rOat1 and between rOct1 and rOct2 (Figure 4, bottom panel). After solubilized His-tagged rOct1 had been mixed with solubilized FLAG-tagged rOat1 and the mixture had been incubated with Ni^{2+}-NTA-agarose beads, 87 ± 5% of FLAG-tagged rOat1 remained in the supernatant and 12 ± 2.5% of FLAG-tagged rOat1 could be eluted from washed beads ($n = 3$ each). The fraction of FLAG-tagged rOat1 which associated with His-tagged rOct1 was much smaller compared to the fraction of FLAG-tagged rOct1 which associated with His-tagged rOct1 ($P < 0.001$). Finally, we tested the association between His-tagged rOct2 and FLAG-tagged rOct1. After LMPG-solubilized His-tagged rOct2, FLAG-tagged rOct1, and Ni^{2+}-NTA-agarose beads had been mixed, 54 ± 8.7% of FLAG-tagged rOct1 remained in the supernatant and 40 ± 9.7% of FLAG-tagged rOct1 could be removed from the washed beads ($n = 3$ each). The association between FLAG-tagged rOct1 and His-tagged rOct2 was weaker compared to that between FLAG-tagged and His-tagged rOct1 ($P < 0.001$); however, a significantly stronger association between rOct1 and rOct2 was observed compared to association between rOct1 and rOat1 ($P < 0.001$). Since the observed strength of association between transporter monomers (rOat1/rOat1 = rOct1/rOct1 > rOct1/rOct2 > rOct1/rOat1) follows the order of primary structure identity (identical amino acids, 67% for rOct1 and rOct2, 33% for rOct1 and rOat1), the observed associations between rOat1 monomers and between rOct1 monomers may have functional implications.

Uptake of Cations by in Vitro Synthesized, Purified, and Reconstituted OCTs. We investigated whether in vitro synthesized and purified rOct1 and rOct2 were functional

[2] Note that during gel chromatography of purified rOat1 in the presence of 1% CHAPS only a relatively small degree of oligomerization was observed (Figure 2A). This is explained by differential effects of 1% CHAPS (gel chromatography in Figure 2A) vs 1% LMPG and 0.5% CHAPS (coprecipitation in Figure 4) on oligomerization (T. Keller and H. Koepsell, unpublished data).

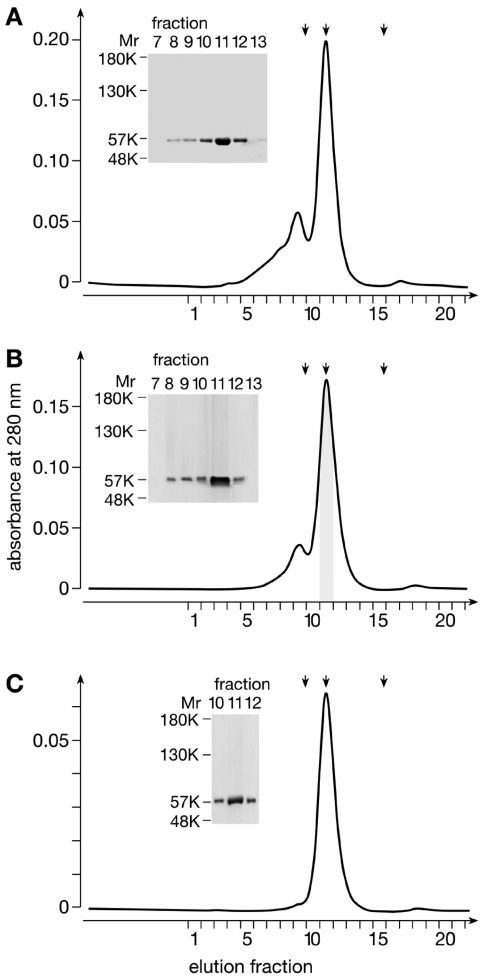

FIGURE 2: Gel chromatography of purified rOat1. Purified FLAG-tagged rOat1 (50 μg) in the presence of 1% CHAPS (A) or 1% octyl glucoside (B) was applied to a Superdex 200 PC 3.2/30 column. The column was equilibrated with Hepes-CHAPS (A) or Hepes-OG (B) and operated at a flow rate of 50 μL/min. Calibration of the column was performed with ribonuclease A (13.7 kDa), bovine serum albumin (67 kDa), and aldolase (158 kDa) (see arrows). In panel C, elution fraction 11 from the chromatography in panel B was rechromatographed. Coomassie-stained SDS−polyacrylamide gels of various elution fractions are shown in the insets. The data suggest purification of rOat1 monomers.

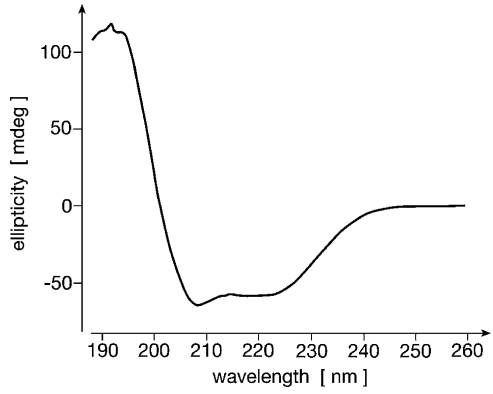

FIGURE 3: CD spectroscopy of purified rOat1. Purified monomeric FLAG-tagged rOat1 (4.8 μmol/L) in 300 μL of sodium phosphate buffer (pH 8) containing 1% octyl glucoside was analyzed by CD spectroscopy. rOat1 was purified as shown in Figure 2C.

after reconstitution. Purified His-tagged rOct1 was reconstituted into large proteoliposomes using a detergent-removal,

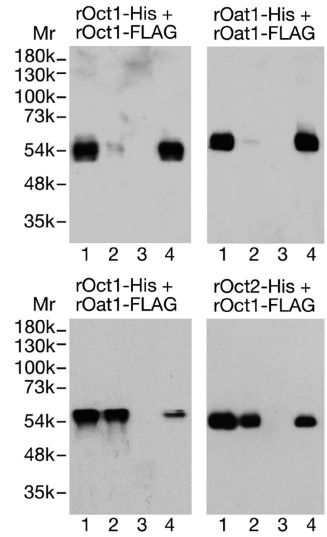

FIGURE 4: Interaction of separately synthesized transporters. In vitro synthesized His-tagged rOat1 (100 μL of LMPG supernatant) was mixed with separately synthesized FLAG-tagged rOat1 (100 μL of LMPG supernatant), His-tagged rOct1 with FLAG-tagged rOct1, His-tagged rOct1 with FLAG-tagged rOat1, and His-tagged rOct2 with FLAG-tagged rOct1. The samples were diluted with an equal volume of Tris buffer containing 1% CHAPS and 10 mM imidazole (lane 1). After incubation for 1 h at 4 °C, 100 μL of a suspension containing Ni^{2+}-NTA-agarose beads was added. The suspension was incubated for 1 h and centrifuged, and the supernatant (lane 2) was removed. The beads were washed and incubated with 1 mL of Hepes-CHAPS containing 20 mM imidazole and pelleted (supernatants, lane 3). His-tagged proteins were eluted by incubating the beads with 400 μL of Hepes-CHAPS containing 100 mM imidazole (lane 4). Proteins were separated by SDS−PAGE, transferred to a blotting membrane, and stained with an antibody against the FLAG tag. Per lane 5 μL was applied.

freeze–thaw procedure. The proteoliposomes loaded with 100 mM potassium cyclamate were preincubated with the potassium ionophore valinomycin. For assessment of MPP^+ uptake, proteoliposomes were incubated with 12 nM [^{3}H]MPP^+ in the presence of 90 mM sodium cyclamate and 10 mM potassium cyclamate. Due to valinomycin and the outwardly directed K^+ gradient, an initial K^+ diffusion potential of approximately −60 mV was generated. MPP^+ uptake was assessed in the absence and presence of 100 μM quinine, and quinine-inhibited uptake was assessed. Figure 5A shows time courses of quinine-inhibited MPP^+ uptake into proteoliposomes which were formed with different amounts of purified rOct1 from the same batch. In proteoliposomes formed after addition of 20 μg of protein, the initial quinine-inhibited MPP^+ uptake rate was linear for 2 s, whereas in proteoliposomes formed after addition of 120 μg of rOct1 protein, initial uptake rates could not be resolved. Organic cation transporters mediate electrogenic organic cation transport that is mainly driven by the membrane potential when small initial gradients of organic cations are applied (*1*). Rapid uptake of MPP^+ into proteoliposomes containing relatively many transporter molecules is supposed to lead to a more rapid dissipation of the K^+ diffusion potential compared to proteoliposomes with fewer transporters, explaining the observed differences in initial MPP^+ uptake rates. To compromise between sufficiently high transport activity in the proteoliposomes and the requirement for measurements of initial linear uptake rates, we routinely performed functional studies with rOct1 and rOct2 using

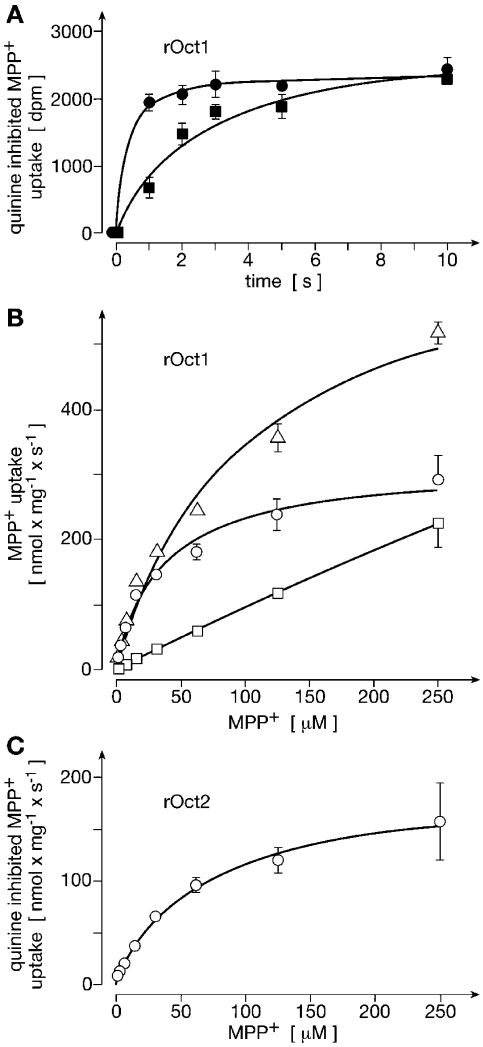

FIGURE 5: Uptake of MPP^+ into proteoliposomes containing purified rOct1 or rOct2. His-tagged rOct1 or rOct2 was expressed in vitro, purified, and reconstituted into proteoliposomes containing 100 mM potassium cyclamate. After preincubation with valinomycin, proteoliposomes were incubated for different time periods with 12 nM [^{3}H]MPP^+ (A) or for 1 s with 12 nM [^{3}H]MPP^+ and various concentrations of nonlabeled MPP^+ (B and C). The incubation buffer contained 90 mM Na^+, 10 mM K^+, and 100 mM $cyclamate^-$. Measurements were performed in the absence and presence of 100 μM quinine, and quinine-inhibited uptake was assessed. (A) Time courses of quinine-inhibited MPP^+ uptake into proteoliposomes containing different amounts of rOct1. Reconstitution was performed with addition of 20 (■) or 120 μg (●) of purified rOct1 protein. (B) Substrate concentration dependence of uptake of MPP^+ into proteoliposomes formed after addition of 60 μg of purified rOct1 protein. Data for MPP^+ uptake in the absence of inhibitors (△), MPP^+ uptake in the presence of quinine (□), and quinine-inhibited MPP^+ uptake (○) are shown. (C) Substrate concentration dependence of quinine-inhibited MPP^+ uptake into proteoliposomes formed with 60 μg of purified rOct2 protein. The Michaelis−Menten equation was fitted to quinine-inhibited MPP^+ uptake in panels B and C.

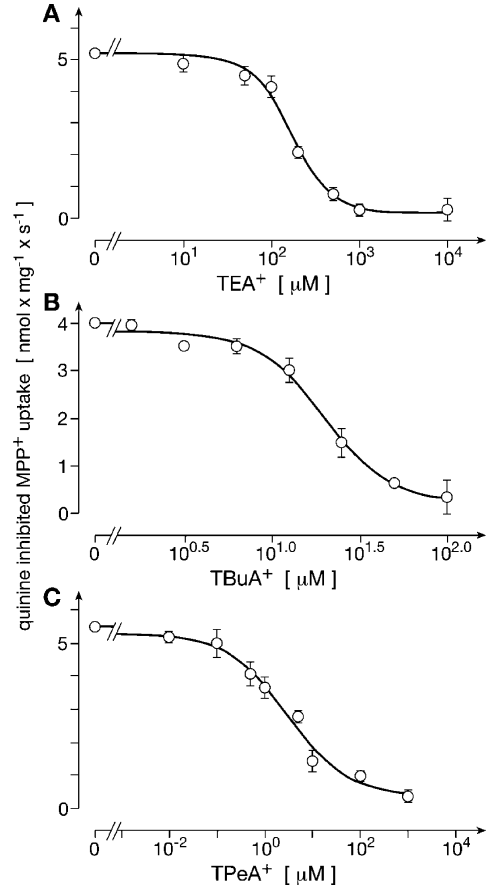

FIGURE 6: Inhibition of uptake of MPP^+ into proteoliposomes containing purified rOct1 by TEA^+, $TBuA^+$, and $TPeA^+$. In vitro expressed and purified His-tagged rOCT1 protein (60 μg) was reconstituted into proteoliposomes containing 100 mM potassium cyclamate. After preincubation with valinomycin in the absence or presence of 100 μM quinine, proteoliposomes were incubated for 1 s with 12 nM [^{3}H]MPP^+ in the presence of 90 mM Na^+, 10 mM K^+, and 100 mM $cyclamate^-$. Incubations were performed in the presence of the indicated concentrations of TEA^+, $TBuA^+$, or $TPeA^+$. Nonspecific uptake measured in the presence of 100 μM quinine was subtracted. Means ± SD of three measurements from individual experiments are shown. Curves were obtained by fitting the Hill equation to the data.

proteoliposomes that were formed after addition of 60 μg of purified protein and measured uptake after a 1 s incubation, a time period showing linear uptake under these conditions (data not shown; see also Figure 2 in ref *23*).

We measured the rate of uptake of [^{3}H]MPP^+ into proteoliposomes containing in vitro synthesized and purified His-tagged rOct1 in the absence and presence of quinine using various concentrations of MPP^+ and calculated the rate of quinine-inhibited MPP^+ uptake (Figure 5B). For quinine-inhibited MPP^+ uptake, hyperbolic saturation curves were obtained that could be fitted with the Michaelis−Menten equation. From three independent experiments, a K_m value of 35 ± 1.5 μM and a V_{max} value of 325 ± 16 nmol mg^{-1} s^{-1} were obtained. These values are not significantly different from the values obtained after reconstitution of purified His-tagged rOct1 that was expressed in Sf9 insect cells (*23*).

To compare cation selectivity of in vitro synthesized rOct1 with rOct1 expressed in Sf9 insect cells, we assessed inhibition of [^{3}H]MPP^+ (12 nM) uptake in the presence of various concentrations of the transported cation TEA^+ or the nontransported inhibitors $TBuA^+$ and $TPeA^+$. From the experiments shown in Figure 6, IC_{50} values of 159 ± 12 μM (TEA^+), 20 ± 1 μM ($TBuA^+$), and 2.9 ± 0.2 μM ($TPeA^+$) were calculated. These values were similar to the values measured under the same experimental conditions in proteoliposomes containing His-tagged rOct1 that was expressed in Sf9 cells (196 μM TEA^+, 19 μM $TBuA^+$, and 1.8 μM $TPeA^+$) (*23*).

We also reconstituted 60 μg of the in vitro expressed and purified His-tagged rOct2 into proteoliposomes and measured the quinine (100 μM)-inhibited uptake of [^{3}H]MPP$^+$ in the presence of various concentrations of nonradioactive MPP$^+$ using the same experimental conditions that were used for rOct1. Quinine-inhibited uptake of MPP$^+$ by rOct2 exhibited a hyperbolic substrate dependence (Figure 5C). A K_m value of 66 $\pm$ 8 μM (n = 3) was calculated which was significantly higher compared to that of rOct1 (P < 0.01). The V_{max} value obtained after reconstitution of rOct2 (194 $\pm$ 9 μmol mg^{-1} s^{-1}) was significantly lower compared to that of rOct1 (P < 0.001).

Characterization of Anion Uptake by in Vitro Synthesized rOat1. We expressed FLAG-tagged rOat1 in vitro, purified the protein using immobilized anti-FLAG antibodies, and reconstituted 60 μg of transporter protein into proteoliposomes. In the first series of experiments, the proteoliposomes were loaded with 100 mM K$^+$, 90 mM cyclamate$^-$, 10 mM Cl$^-$, and 0.5 mM α-ketoglutarate (KG^{2-}) and incubated with 5 μM [^{14}C]PAH$^-$ in the presence of 100 mM KCl (Figure 7). To correct for nonspecific uptake, the measurements were performed in the absence and presence of 2 mM probenecid, an inhibitor of OATs. Under these conditions, with initial gradients of 90 mM Cl$^-$ (out > in) and 0.5 mM KG^{2-} (in > out), we expected optimal transport activity according to previously reported PAH$^-$ uptake measurements in OAT1-transfected cells (*25, 26, 33, 34*). Measuring the time course of PAH$^-$ uptake, we observed that probenecid-inhibited PAH$^-$ uptake was linear for 90 s (Figure 7A). Using the same experimental conditions with an incubation time of 90 s, we measured the substrate dependence of uptake of [^{14}C]PAH$^-$ in the absence (△) and presence (□) of probenecid (Figure 7B) and calculated the probenecid-inhibited [^{14}C]PAH$^-$ uptake (Figure 7C). Fitting the Michaelis−Menten equation to probenecid-inhibited [^{14}C]PAH$^-$ uptake in this experiment yielded an estimated apparent K_m value of 73 $\pm$ 10 μM (SE). Using slightly different experimental conditions [initial gradients of 100 mM Cl$^-$ (out > in) and 0.5 mM KG^{2-} (in > out), clamped membrane potential], a K_m value of 74 $\pm$ 1.2 μM (SD; n = 3) was obtained (see below). These K_m values are similar to the K_m value of 70 μM determined after expression of rOat1 in oocytes of *X. laevis* (*25*).

In Figure 8A, we investigated whether the initial outwardly directed gradient of 0.5 mM KG^{2-} is necessary to observe rOat1-mediated PAH$^-$ uptake in proteoliposomes, which has been reported for rOat1-mediated uptake of PAH$^-$ in *X. laevis* oocytes (*25, 26*). This was the case; the rate of probenecid-inhibited uptake of 5 μM PAH$^-$ into the proteoliposomes measured in the presence of an outwardly directed, initial gradient of 0.5 mM KG^{2-} was 15 times higher compared to the rate of PAH$^-$ uptake measured with 0.5 mM KG^{2-} on both sides of the membrane (P < 0.001). To exclude the possibility that KG^{2-} efflux generates an outside negative diffusion potential because it is electrogenic and thereby stimulates electrogenic PAH$^-$ uptake, we performed the same experiment under voltage clamp conditions. This was achieved by preincubating the proteoliposomes (100 mM K$^+$ inside and outside) with the potassium ionophore valinomycin. Since valinomycin had no effect on the *trans* stimulation of PAH$^-$ uptake by KG^{2-} (Figure 8A), an indirect stimulation of PAH$^-$ uptake via the membrane potential can be ruled out.

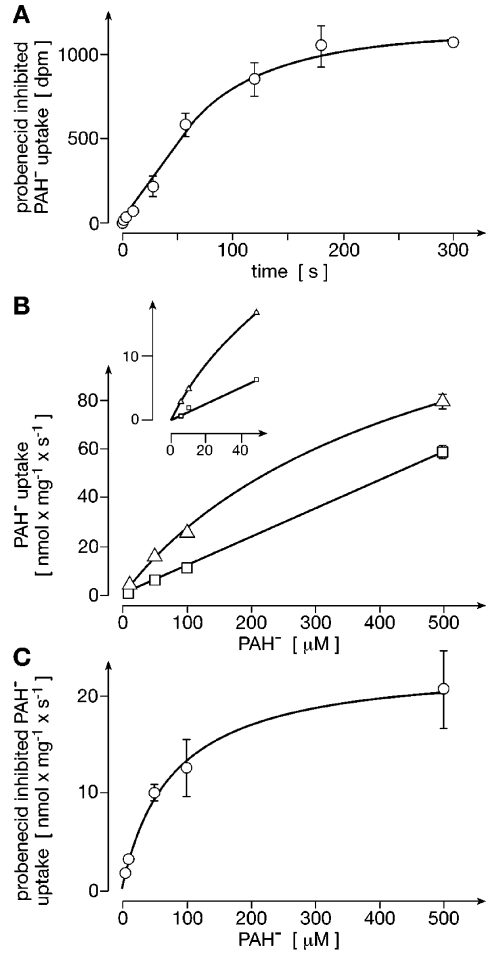

FIGURE 7: Time course and substrate dependence of uptake of PAH$^-$ into proteoliposomes containing purified rOat1. In vitro expressed and purified His-tagged rOat1 protein (60 μg) was incorporated into proteoliposomes containing 100 mM K$^+$, 90 mM cyclamate$^-$, 10 mM Cl$^-$, and 0.5 mM α-ketoglutarate (KG^{2-}). Proteoliposomes were incubated with 100 mM KCl containing [^{14}C]PAH$^-$ in the absence and presence of 2 mM probenecid. (A) Probenecid-inhibited uptake of 5 μM [^{14}C]PAH$^-$ measured after different incubation times. (B) [^{14}C]PAH$^-$ uptake after a 90 s incubation measured in the presence of different PAH$^-$ concentrations in the absence (△) and presence (□) of probenecid. The inset shows a larger magnification of uptake rates at low PAH$^-$ concentrations. (C) Probenecid-inhibited [^{14}C]PAH$^-$ uptake calculated from the measurements in Figure 7B. The Michaelis−Menten equation was fitted to these data.

Next we investigated whether rOAT1-mediated PAH$^-$ uptake in proteoliposomes is stimulated by chloride as described previously for hOat1 expressed in cells (*33–35*). Purified His-tagged rOat1 was reconstituted into proteoliposomes that contained 100 mM K$^+$, 0.5 mM KG^{2-}, and either 100 mM cyclamate$^-$ or 100 mM Cl$^-$, or mixtures of cyclamate$^-$ and Cl$^-$. After preincubation with valinomycin, the rate of uptake of 5 μM [^{14}C]PAH$^-$ was measured in the presence of 100 mM K$^+$ and either 100 mM cyclamate$^-$, 100 mM Cl$^-$, or various mixtures of both anions (Figure 8B,C). In the absence of Cl$^-$, PAH$^-$ uptake was 50% slower than PAH$^-$ uptake measured in the presence of 100 mM Cl$^-$ in transport buffer. With 10 mM Cl$^-$ on both sides of the membrane, PAH$^-$ uptake was similar to that in the absence of Cl$^-$ (Figure 8B). So far, the data are consistent with activation at a low-affinity chloride activation site as well as with cotransport of PAH$^-$ and Cl$^-$ in exchange for KG^{2-}.

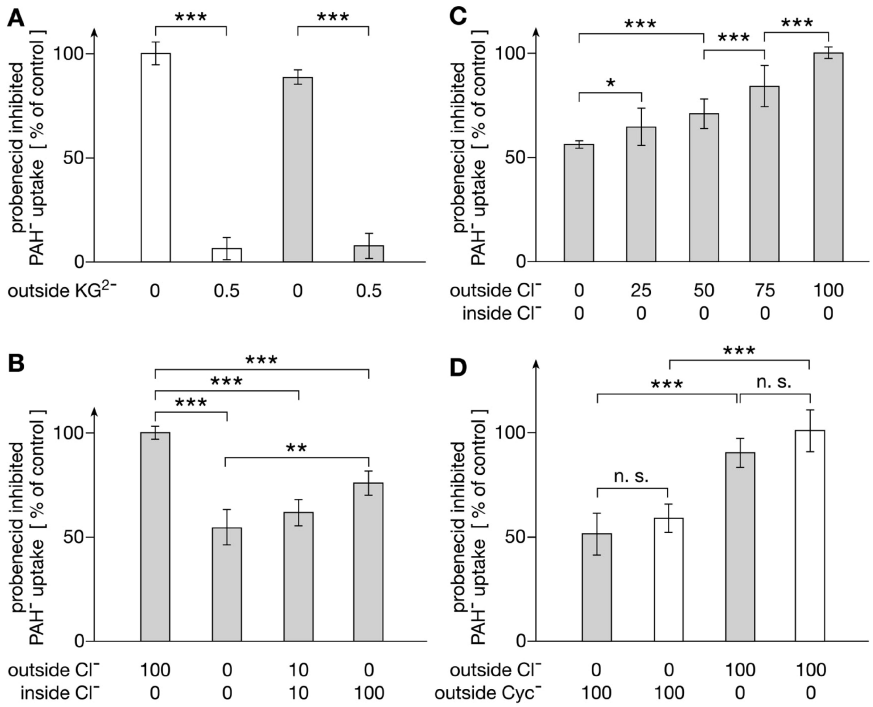

FIGURE 8: Functional characterization of PAH^- uptake by rOat1 in proteoliposomes. Purified His-tagged rOat1 protein (60 μg) expressed in vitro was reconstituted into proteoliposomes in the presence of different anions. Before uptake measurements were started, proteoliposomes were preincubated without (white columns) and with valinomycin (gray columns). For uptake measurements, they were incubated for 90 s with 5 μM [^{14}C]PAH^- in the absence and presence of 2 mM probenecid. The incubation buffer contained different concentrations of anions and cations. Probenecid-inhibited uptake was calculated. (A) *trans* stimulation of PAH^- uptake by 0.5 mM α-ketoglutarate (KG^{2-}). The proteoliposomes contained 100 mM K^+, 90 mM cyclamate$^-$, 10 mM Cl^-, and 0.5 mM KG^{2-}. They were incubated with [^{14}C]PAH^- in the presence of 100 mM KCl or 100 mM KCl with 0.5 mM KG^{2-}. (B) Stimulation of rOat1-mediated PAH^- uptake by chloride. Proteoliposomes contained 100 mM K^+, 0.5 mM KG^{2-}, and 100 mM anions (cyclamate$^-$ and Cl^-). For uptake measurements, proteoliposomes were incubated with [^{14}C]PAH^- in the presence of 100 mM K^+ and 100 mM anions (cyclamate$^-$ and Cl^-). The concentrations of Cl^- (in millimolar) are indicated. (C) Effect of chloride concentration on PAH^- uptake. The experiment was performed, and the data are presented as in panel B. (D) No effect of membrane potential on PAH^- uptake in the absence and presence of chloride. The proteoliposomes contained 100 mM K^+, 100 mM cyclamate$^-$, and 0.5 mM KG^{2-}. For uptake measurement, proteoliposomes were incubated with PAH^- in the presence of 100 mM Na^+ and either 100 mM cyclamate$^-$ (Cyc^-) or 100 mM Cl^-. Concentrations of KG^{2-}, Cl^-, and Cyc^- are given in millimolar. One asterisk indicates a P of <0.05, two asterisks indicate a P of <0.01, and three a P of <0.001. n.s. means not significant. The data indicate potential-independent *trans* stimultation of rOat1-mediated PAH^- uptake by KG^{2-} that is stimulated by low-affinity interaction of Cl^- with a modifier site.

However, the observation that PAH^- uptake measured in the presence of an initial outwardly directed gradient of 100 mM Cl^- was significantly higher compared to PAH^- uptake measured in the absence of Cl^- (Figure 8B) is in contradiction with the latter interpretation. In Figure 8C, [^{14}C]PAH^- uptake was measured in the presence of different concentrations of Cl^- in incubation buffer, trying to evaluate the affinity of the observed effect of Cl^- on PAH^- transport. PAH^- uptake increased with increasing chloride concentrations; however, it did not reach saturation within the employed concentration range between 0 and 100 mM. The data are consistent with binding of chloride to a low-affinity activation site of rOat1.

Additional experiments were performed trying to validate our interpretation that Cl^- interacts with a modifier site rather than being cotransported with PAH^-. Since direct low-affinity uptake of Cl^- into proteoliposomes cannot be resolved for technical reasons, we reasoned that cotransport of Cl^- with PAH^- should be detectable via a Cl^--induced change in the potential dependence of PAH^- uptake. Proteoliposomes containing 100 mM potassium cyclamate and 0.5 mM KG^{2-} were preincubated without or with valinomycin, and uptake of [^{14}C]PAH into proteoliposomes was measured in the presence of 100 mM sodium cyclamate or 100 mM NaCl (Figure 8D). Regardless of whether uptake was measured without or with an inwardly directed Cl^- gradient, no significant effects of valinomycin were observed. Since the potassium diffusion potential did not alter PAH uptake under either condition, the data strongly suggest that Cl^- is not cotransported with PAH^- and that PAH^- uptake in the presence of a *trans* gradient of KG^{2-} is electroneutral.

We also compared substrate activation of PAH^- uptake *trans*-stimulated by KG^{2-} in the absence of chloride and in the presence of an inwardly directed Cl^- gradient of initially 100 mM. With the Cl^- gradient, the V_{max} was significantly higher than that without a chloride gradient [22.9 ± 2.9 and 14.7 ± 2.3 pmol mg^{-1} s^{-1}, respectively (n = 3 each, P < 0.05)]. At variance, the apparent K_m was not changed (73.5 ± 1.1 μM with the Cl^- gradient vs 73.0 ± 4.6 μM without the Cl^- gradient).

To distinguish whether the observed *trans* stimulation of PAH^- uptake by KG^{2-} is due to activation of rOat1 via a modifier site or whether rOat1 is a PAH^-/KG^{2-} antiporter, we investigated whether an outwardly directed KG^{2-} gradient is able to induce an "overshoot", i.e., whether it increases the intravesicular PAH^- concentration transiently above the equilibrium concentration of PAH^-; 300 μg of in vitro expressed and purified FLAG-tagged rOat1 was reconstituted into proteoliposomes containing 100 mM potassium cycla-

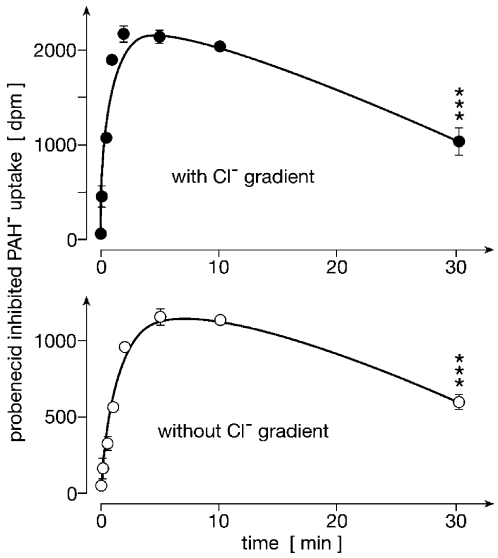

FIGURE 9: Demonstration of PAH^-/KG^{2-} antiport by rOat1 in proteoliposomes containing purified rOat1. Purified FLAG-tagged rOat1 protein (300 μg) expressed in vitro was reconstituted into proteoliposomes containing 100 mM potassium cyclamate and 0.5 mM KG^{2-}. After preincubation with valinomycin, probenecid-inhibited uptake of 5 μM [^{14}C]PAH^- into proteoliposomes was measured after incubation for various time periods in the presence of either 100 mM potassium chloride (top panel) or 100 mM potassium cyclamate (bottom panel). Three asterisks indicate a P of <0.001 for the difference from PAH^- uptake after incubation for 2–10 min. The obtained overshoot indicates that rOat1 is a PAH^-/KG^{2-} antiporter.

mate and 0.5 mM KG^{2-}. Proteoliposomes were preincubated with valinomycin. For uptake measurements, proteoliposomes were incubated for various time intervals with 5 μM [^{14}C]PAH^- in the presence of 100 mM potassium chloride (Figure 9, top panel) or 100 mM potassium cyclamate (Figure 9, bottom panel). Between 2 and 10 min after incubation with [^{14}C]PAH^-, the concentration of [^{14}C]PAH^- within the proteoliposomes was significantly higher than the concentration after incubation for 30 min ($P < 0.001$). The data indicate that rOat1 is an obligatory-coupled PAH^-/KG^{2-} antiporter.

DISCUSSION

In this paper, we describe CF expression and functional active reconstitution of three polyspecific drug transporters from the *SLC22* transporter family that belongs to the major facilitator superfamily (*36*). From 1 mL reaction vessels, 0.16–0.36 mg of pure functional active transporter proteins was obtained. Using 5–10 reaction vessels, sufficient amounts of the transporter proteins for crystallization attempts and for biophysical characterizations can be obtained at relatively low cost within 3 days. Freeze–thaw reconstitution of purified proteins into large cholesterol-rich proteoliposomes allowed functional characterization of electrogenic organic cation transporters and an electroneutral organic anion exchanger. Since in proteoliposomes ion and substrate composition can be controlled on both sides of the membrane, more unambiguous functional characterization can be performed than after expression of the transporters in cells. For example, in this study we provide experimental evidence that rOat1 is an obligatory electroneutral PAH^-/dicarboxylic antiporter that is stimulated by Cl^- binding to a low-affinity activation site.

Cell Free Expression. Since 2003, CF expression with similar yields has been reported for various integral membrane proteins. The synthesized integral membrane proteins include transporters and channels from *E. coli* with 2–10 transmembrane α-helices (TMHs) (*27, 37, 38*), the β-barrel nucleoside transporter Tsx from *E. coli* (*39*), and several G-protein-coupled receptors (GPCRs) with seven TMHs from human (*40, 41*). CF synthesis has been performed in the absence of detergent like in this study, but also in the presence of detergent or in the presence of liposomes that may allow oriented protein insertion (*42*). The yields of synthesized proteins varied between 10 μg and 4 mg of protein per 1 mL reaction volume, showing a reverse correlation between the molecular weight of the synthesized protein and yield (*39, 43*). rOct1, rOct2, and rOat1 are the first eukaryotic transporters that have been synthesized in a CF system. The monomers of rOct1, rOct2, and rOat1 belong to the largest proteins of CF-expressed integral membrane proteins. They are the first proteins with 12 TMHs that were obtained in high yield.

Reconstitution. Functional activity of CF-expressed integral membrane proteins has been only demonstrated in the following cases: (a) channel activity of the mechanosensitive channel MscL from *E. coli* (136 aa long, two TMHs) using patch-clamp of giant proteoliposomes (*38, 44*), (b) channel activity of the β-barrel nucleoside transporter Tsx from *E. coli* (272 aa long) observed in black lipid membranes (*39*), (c) uptake of fluorescent or radioactively labeled substrate into proteoliposomes containing the small (100 aa long, four TMHs) multidrug transporter EmrE from *E. coli* (*27, 37*), (d) ligand binding of immobilized human GPCR receptors β2 adrenergic receptor (*40*) and endothelin B (*41*), and (e) photocycle activity of bacteriorhodopsin that was inserted into liposomes during CF synthesis and attached to a black lipid membrane (*42*).

To measure organic cation uptake by transporters rOct1 and rOct2 that are driven by substrate gradient and membrane potential (*3, 11, 45*) and uptake of PAH^- by rOat1 that was only observed in the presence of a *trans*-KG^{2-} gradient (*2, 25, 26*), we reconstituted the transporters into large cholesterol-rich proteoliposomes with diameters between 0.5 and 2 μm (*30, 46*). The employed reconstitution protocol had been optimized to analyze transport activities of electrogenic Na^+ cotransporters (*46, 47*). Because of their relatively large size and low passive permeability, these proteoliposomes are well suited to measurement of initial uptake rates of transporters that are driven by ion gradients, i.e., cotransporters or antiporters. With the help of K^+ gradients and valinomycin, potassium diffusion potentials can be generated that provide the driving force for electrogenic transporters. After reconstitution of rOct1 expressed in insect cells, we previously showed that these proteoliposomes can be used to measure organic cation uptake driven by a valinomycin-induced inside negative diffusion potential (*23*). For such measurements, the amount of transporter molecules per proteoliposome must be kept small to prevent the possibility that the outside positive diffusion potential generated by valinomycin-mediated potassium efflux is compromised by transporter-mediated uptake of positive charge and to ensure that the potential-driven uptake of organic cation substrate is slow enough to allow detection of an initial linear concentration increase in organic cations

in the proteoliposomes. Figure 5A shows that the time period of linear MPP^+ uptake by rOct1 was decreased dramatically when the amount of reconstituted transporter was increased. So far, the orientations of rOct1, rOct2, and rOat1 in the proteoliposmes have not been determined. Since rOct1 and rOct2 mediate electrogenic organic cation transport in both directions across the plasma membrane showing similar K_m values (*1, 12*) and also rOat1 is supposed to operate similarly in both directions (*2*), the orientation of the transporters in the proteoliposomes is not supposed to influence the functional properties described in this paper.

Functional Properties of CF-Expressed Organic Cation Transporters. After reconstitution of CF-expressed rOct1 or rOct2, quinine inhibitable uptake of MPP^+ was demonstrated showing saturation kinetics. The data show that glycosylation at the large extracellular loop (*3*) is not required for transport activity. Fitting the Michaelis−Menten equation to the data yielded K_m values that show less variation compared to uptake measurements with overexpressing cell lines. This allowed detection of a significantly lower K_m value for MPP^+ uptake by rOct1 versus rOct2. Comparing properties of reconstituted rOct1 purified from Sf9 insect cells versus rOct1 purified after CF expression, we found virtually the same K_m values and the same V_{max} values per milligram for MPP^+ uptake. We also observed identical affinities for inhibition of MPP^+ uptake by substrate TEA^+ and the two nontransported inhibitors $TBuA^+$ and $TPeA^+$. This indicates that a similar native tertiary structure of rOct1 is obtained after CF synthesis in the absence of detergent compared to purification of rOct1 from insect cells.

Comparing functional properties of rOct1 observed after expression in human embryonic kidney (HEK) 293 cells or oocytes with those obtained in proteoliposomes, similar affinities for the organic cation substrates MPP^+ and TEA^+ were obtained, however, we observed significantly different affinities for the nontransported inhibitors $TBuA^+$ and $TPeA^+$. The K_m values determined for MPP^+ uptake in proteoliposomes and HEK293 cells were 33 ± 11 μM ($n = 6$) and 14 ± 4 μM ($n = 3$), respectively. The IC_{50} values determined for inhibition of MPP^+ uptake by TEA^+ measured in proteoliposomes and HEK293 cells were 66 ± 8 μM ($n = 3$) and 58 ± 21 μM ($n = 4$; H. Koepsell et al., unpublished data), respectively. At variance, in proteoliposomes containing rOct1 or HEK293 cells expressing rOct1, 17- or 10-fold lower affinities, respectively, for inhibition of MPP^+ uptake by TBuA and TPeA were obtained [TBuA, 19 ± 0.5 μM ($n = 2$) vs 1.1 ± 0.1 μM ($n = 3$); TPeA, 2.8 ± 0.1 μM ($n = 2$) vs 0.28 ± 0.06 μM ($n = 5$) (this study, ref *23*, and unpublished data of H. Koepsell)]. The differences in affinity for $TBuA^+$ and $TPeA^+$ in proteoliposomes versus HEK293 cells indicate differences in configuration of the substrate binding region. These differences may have various causes. For example, they could be due to different lipid environments, to different regulatory states, or to binding of additional unidentified ligands in cells. The differences in affinity cannot be explained by a differentially oriented incorporation of rOct1 into the liposomal bilayer compared to the plasma membrane of HEK293 cells. A reverse orientation of rOct1 in proteoliposomes compared to HEK293 cells may contribute to the decrease in affinity for $TBuA^+$ but not for $TPeA^+$ since $TBuA^+$ has a 4-fold higher and TPeA a 2-fold lower affinity for the outward-facing substrate binding pocket compared to the inward-facing pocket (*14*) (H. Koepsell, unpublished data). The unchanged affinity for transported cations and decreased affinity for nontransported inhibitors support the concept that rOct1 contains a complex substrate binding region with partially overlapping and allosterically interacting binding sites for different cations (*19, 22*).

Functional Properties of rOat1. Functional reconstitution of CF-expressed rOat1 into proteoliposomes showed that glycosylation of the large extracellular loop is not required for functional activity and does not change the K_m value for PAH^- uptake. Importantly, it provided new insight into the functional mechanism of rOat1. Previous experiments with oocytes showed that PAH^- uptake by rOat1 is *trans* stimulated by KG^{2-}, and it was proposed that rOat1 is a PAH^-/KG^{2-} antiporter (*25, 26*). Pioneering studies with membrane vesicles from basolateral membranes of renal proximal tubules had indicated that PAH^- uptake is indirectly coupled to a secondary active sodium dicarboxylate cotransporter (*48, 49*). It was shown that PAH^- uptake into vesicles was *trans* stimulated by KG^{2-} and that the intravesicular PAH^- concentration increased above the equilibrium value (overshoot phenomenon) when an inwardly directed sodium gradient was applied and KG^{2-} was present in the medium, or when the vesicles were preloaded with KG^{2-}. With regard to the stoichiometry and voltage dependence of PAH^-/KG^{2-} exchange in vesicles, contradictory results were reported (*49–51*). In addition, it remained unclear whether the data obtained from vesicle studies had to be attributed to OAT1 or to organic anion transporter OAT3 that is located in the same membrane. Measurements of the electrical properties or of the PAH^-/KG^{2-} stoichiometry of OAT1 expressed in cells were handicapped by high membrane conductances for chloride and potential effects of additional intracellular substrates.

Using proteoliposomes, we provided evidence that rOat1 is an electroneutral obligatory PAH^-/KG^{2-} exchanger rather than an electrogenic facilitative diffusion system that is *trans* stimulated by intracellular dicarboxylates. Excluding indirect coupling via the membrane potential, we observed that an in > out gradient of KG^{2-} was able to increase the PAH^- concentration within proteoliposomes above equilibrium in a manner independent of chloride (Figure 9). Since the "PAH^- overshoot" measured under voltage clamp conditions cannot be obtained by the two-step molecular mechanism, PAH^- uptake followed by KG^{2-} efflux, it provides evidence for an obligatory PAH^-/KG^{2-} antiporter. We also investigated the role of chloride. Stimulation of PAH^- uptake by chloride was first demonstrated in membrane vesicles (*52, 53*). Using oocytes expressing hOAT1, HEK293 cells expressing hOAT1, or HEK293 cells expressing hOAT3, stimulation of anion transport by chloride was observed (*17, 33–35*). Whereas Cl^- increased the V_{max} of hOAT1 without altering the amount of transporter within the membrane, it decreased the K_m of hOAT3 (*17, 35*). In these studies, it could not be distinguished whether Cl^- is cotransported with PAH^- or whether Cl^- modifies transport activity or affinity without being translocated itself. Using proteoliposomes, we answered this question for rOat1, providing evidence that Cl^- acts as a nontransported modifier. We observed that the V_{max} of rOat1-mediated PAH^-/KG^{2-} antiport is stimulated in the presence of 100 mM extracellular Cl^- versus $cyclamate^-$. Cotransport

of Cl^- was ruled out by showing that (a) the stimulation by Cl^- was independent of Cl^- gradients and (b) neither PAH^-/KG^{2-} antiport in the absence of Cl^- nor PAH^-/KG^{2-} antiport in the presence of an inwardly directed Cl^- gradient was stimulated by an outwardly directed potassium diffusion potential. Missing stimulation by an inward negative membrane potential in the absence of anions other than cyclamate$^-$ strongly suggests electroneutral exchange of two PAH^- against one KG^{2-}.

In summary, we reported CF expression of functionally active rOct1, rOct2, and rOat1 that allows biophysical characterization and crystallization of these transporters. Using reconstituted rOat1, we provided evidence that rOat1 is an electroneutral obligatory PAH^-/KG^{2-} antiporter that is stimulated by low-affinity binding of chloride to an extracellular modifier site.

ACKNOWLEDGMENT

We thank Christian Gerum (Institute of Organic Chemistry and Chemical Biology, University of Frankfurt) for performing the CD analysis, Dr. Gerhard Burckhardt (Institute of Physiology and Pathophysiology, University of Göttingen) for expert advice, and Michael Christof for preparing the figures.

REFERENCES

1. Koepsell, H., Schmitt, B. M., and Gorboulev, V. (2003) Organic cation transporters. *Rev. Physiol. Biochem. Pharmacol. 150*, 36–90.
2. Rizwan, A. N., and Burckhardt, G. (2007) Organic anion transporters of the SLC22 family: Biopharmaceutical, physiological, and pathological roles. *Pharm. Res. 24*, 450–470.
3. Koepsell, H., Lips, K., and Volk, C. (2007) Polyspecific organic cation transporters: Structure, function, physiological roles, and biopharmaceutical implications. *Pharm. Res. 24*, 1227–1251.
4. Nezu, J.-i., Tamai, I., Oku, A., Ohashi, R., Yabuuchi, H., Hashimoto, N., Nikaido, H., Sai, Y., Koizumi, A., Shoji, Y., Takada, G., Matsuishi, T., Yoshino, M., Kato, H., Ohura, T., Tsujimoto, G., Hayakawa, J.-i., Shimane, M., and Tsuji, A. (1999) Primary systemic carnitine deficiency is caused by mutations in a gene encoding sodium ion-dependent carnitine transporter. *Nat. Genet. 21*, 91–94.
5. Wang, Y., Ye, J., Ganapathy, V., and Longo, N. (1999) Mutations in the organic cation/carnitine transporter OCTN2 in primary carnitine deficiency. *Proc. Natl. Acad. Sci. U.S.A. 96*, 2356–2360.
6. Tokuhiro, S., Yamada, R., Chang, X., Suzuki, A., Kochi, Y., Sawada, T., Suzuki, M., Nagasaki, M., Ohtsuki, M., Ono, M., Furukawa, H., Nagashima, M., Yoshino, S., Mabuchi, A., Sekine, A., Saito, S., Takahashi, A., Tsunoda, T., Nakamura, Y., and Yamamoto, K. (2003) An intronic SNP in a RUNX1 binding site of SLC22A4, encoding an organic cation transporter, is associated with rheumatoid arthritis. *Nat. Genet. 35*, 341–348.
7. Peltekova, V. D., Wintle, R. F., Rubin, L. A., Amos, C. I., Huang, Q., Gu, X., Newman, B., Van Oene, M., Cescon, D., Greenberg, G., Griffiths, A. M., George-Hyslop, P. H., and Siminovitch, K. A. (2004) Functional variants of OCTN cation transporter genes are associated with Crohn disease. *Nat. Genet. 36*, 471–475.
8. Nakamura, N., Masuda, S., Takahashi, K., Saito, H., Okuda, M., and Inui, K.-I. (2004) Decreased expression of glucose and peptide transporters in rat remnant kidney. *Drug Metab. Pharmacokinet. 19*, 41–47.
9. Shu, Y., Sheardown, S. A., Brown, C., Owen, R. P., Zhang, S., Castro, R. A., Ianculescu, A. G., Yue, L., Lo, J. C., Burchard, E. G., Brett, C. M., and Giacomini, K. M. (2007) Effect of genetic variation in the organic cation transporter 1 (OCT1) on metformin action. *J. Clin. Invest. 117*, 1422–1431.
10. Wang, L., Giannoudis, A., Lane, S., Williamson, P., Pirmohamed, M., and Clark, R. E. (2008) Expression of the uptake drug transporter hOCT1 is an important clinical determinant of the response to imatinib in chronic myeloid leukemia. *Clin. Pharmacol. Ther. 83*, 258–264.
11. Gründemann, D., Gorboulev, V., Gambaryan, S., Veyhl, M., and Koepsell, H. (1994) Drug excretion mediated by a new prototype of polyspecific transporter. *Nature 372*, 549–552.
12. Budiman, T., Bamberg, E., Koepsell, H., and Nagel, G. (2000) Mechanism of electrogenic cation transport by the cloned organic cation transporter 2 from rat. *J. Biol. Chem. 275*, 29413–29420.
13. Schmitt, B. M., and Koepsell, H. (2005) Alkali cation binding and permeation in the rat organic cation transporter rOCT2. *J. Biol. Chem. 280*, 24481–24490.
14. Volk, C., Gorboulev, V., Budiman, T., Nagel, G., and Koepsell, H. (2003) Different affinities of inhibitors to the outwardly and inwardly directed substrate binding site of organic cation transporter 2. *Mol. Pharmacol. 64*, 1037–1047.
15. Wolff, N. A., Grünwald, B., Friedrich, B., Lang, F., Godehardt, S., and Burckhardt, G. (2001) Cationic amino acids involved in dicarboxylate binding of the flounder renal organic anion transporter. *J. Am. Soc. Nephrol. 12*, 2012–2018.
16. Wang, Y., Meadows, T. A., and Longo, N. (2000) Abnormal sodium stimulation of carnitine transport in primary carnitine deficiency. *J. Biol. Chem. 275*, 20782–20786.
17. Rizwan, A. N., Krick, W., and Burckhardt, G. (2007) The chloride dependence of the human organic anion transporter 1 (hOAT1) is blunted by mutation of a single amino acid. *J. Biol. Chem. 282*, 13402–13409.
18. Abramson, J., Smirnova, I., Kasho, V., Verner, G., Kaback, H. R., and Iwata, S. (2003) Structure and mechanism of the lactose permease of *Escherichia coli*. *Science 301*, 610–615.
19. Popp, C., Gorboulev, V., Müller, T. D., Gorbunov, D., Shatskaya, N., and Koepsell, H. (2005) Amino acids critical for substrate affinity of rat organic cation transporter 1 line the substrate binding region in a model derived from the tertiary structure of lactose permease. *Mol. Pharmacol. 67*, 1600–1611.
20. Zhang, X., Shirahatti, N. V., Mahadevan, D., and Wright, S. H. (2005) A conserved glutamate residue in transmembrane helix 10 influences substrate specificity of rabbit OCT2 (SLC22A2). *J. Biol. Chem. 280*, 34813–34822.
21. Sturm, A., Gorboulev, V., Gorbunov, D., Keller, T., Volk, C., Schmitt, B. M., Schlachtbauer, P., Ciarimboli, G., and Koepsell, H. (2007) Identification of cysteines in rat organic cation transporters rOCT1 (C322, C451) and rOCT2 (C451) critical for transport activity and substrate affinity. *Am. J. Physiol. 293*, F767–F779.
22. Gorbunov, D., Gorboulev, V., Shatskaya, N., Mueller, T., Bamberg, E., Friedrich, T., and Koepsell, H. (2008) High-affinity cation binding to organic cation transporter 1 induces movement of helix 11 and blocks transport after mutations in a modeled interaction domain between two helices. *Mol. Pharmacol. 73*, 50–61.
23. Keller, T., Elfeber, M., Gorboulev, V., Reiländer, H., and Koepsell, H. (2005) Purification and functional reconstitution of the rat organic cation transporter OCT1. *Biochemistry 44*, 12253–12263.
24. Okuda, M., Saito, H., Urakami, Y., Takano, M., and Inui, K. (1996) cDNA cloning and functional expression of a novel rat kidney organic cation transporter, OCT2. *Biochem. Biophys. Res. Commun. 224*, 500–507.
25. Sweet, D. H., Wolff, N. A., and Pritchard, J. B. (1997) Expression cloning and characterization of rOAT1, the basolateral organic anion transporter in rat kidney. *J. Biol. Chem. 272*, 30088–30095.
26. Sekine, T., Watanabe, N., Hosoyamada, M., Kanai, Y., and Endou, H. (1997) Expression cloning and characterization of a novel multispecific organic anion transporter. *J. Biol. Chem. 272*, 18526–18529.
27. Klammt, C., Löhr, F., Schäfer, B., Haase, W., Dötsch, V., Rüterjans, H., Glaubitz, C., and Bernhard, F. (2004) High level cell-free expression and specific labeling of integral membrane proteins. *Eur. J. Biochem. 271*, 568–580.
28. Rohl, C. A., and Baldwin, R. L. (1997) Comparison of NH exchange and circular dichroism as techniques for measuring the parameters of the helix-coil transition in peptides. *Biochemistry 36*, 8435–8442.
29. Rost, B. (1996) PHD: Predicting one-dimensional protein structure by profile-based neural networks. *Methods Enzymol. 266*, 525–539.
30. Koepsell, H., and Seibicke, S. (1990) Reconstitution and fractionation of renal brush border transport proteins. *Methods Enzymol. 191*, 583–605.
31. Valentin, M., Kühlkamp, T., Wagner, K., Krohne, G., Arndt, P., Baumgarten, K., Weber, W.-M., Segal, A., Veyhl, M., and Koepsell, H. (2000) The transport modifier RS1 is localized at the inner side of the plasma membrane and changes membrane capacitance. *Biochim. Biophys. Acta 1468*, 367–380.

32. Korn, T., Kühlkamp, T., Track, C., Schatz, I., Baumgarten, K., Gorboulev, V., and Koepsell, H. (2001) The plasma membrane-associated protein RS1 decreases transcription of the transporter SGLT1 in confluent LLC-PK1 cells. *J. Biol. Chem. 276*, 45330–45340.
33. Race, J. E., Grassl, S. M., Williams, W. J., and Holtzman, E. J. (1999) Molecular cloning and characterization of two novel human renal organic anion transporters (hOAT1 and hOAT3). *Biochem. Biophys. Res. Commun. 255*, 508–514.
34. Hosoyamada, M., Sekine, T., Kanai, Y., and Endou, H. (1999) Molecular cloning and functional expression of a multispecific organic anion transporter from human kidney. *Am. J. Physiol. 276*, F122–F128.
35. Ueo, H., Motohashi, H., Katsura, T., and Inui, K.-i. (2007) Cl-Dependent up-regulation of human organic anion transporters: Different effects on transport kinetics between hOAT1 and hOAT3. *Am. J. Physiol. 293*, F391–F397.
36. Pao, S. S., Paulsen, I. T., and Saier, M. H., Jr. (1998) Major facilitator superfamily. *Microbiol. Mol. Biol. Rev. 62*, 1–34.
37. Elbaz, Y., Steiner-Mordoch, S., Danieli, T., and Schuldiner, S. (2004) In vitro synthesis of fully functional EmrE, a multidrug transporter, and study of its oligomeric state. *Proc. Natl. Acad. Sci. U.S.A. 101*, 1519–1524.
38. Berrier, C., Park, K.-H., Abes, S., Bibonne, A., Betton, J.-M., and Ghazi, A. (2004) Cell-free synthesis of a functional ion channel in the absence of a membrane and in the presence of detergent. *Biochemistry 43*, 12585–12591.
39. Klammt, C., Schwarz, D., Fendler, K., Haase, W., Dötsch, V., and Bernhard, F. (2005) Evaluation of detergents for the soluble expression of α-helical and *β*-barrel-type integral membrane proteins by a preparative scale individual cell-free expression system. *FEBS J. 272*, 6024–6038.
40. Ishihara, G., Goto, M., Saeki, M., Ito, K., Hori, T., Kigawa, T., Shirouzu, M., and Yokoyama, S. (2005) Expression of G protein coupled receptors in a cell-free translational system using detergents and thioredoxin-fusion vectors. *Protein Expression Purif. 41*, 27–37.
41. Klammt, C., Schwarz, D., Eifler, N., Engel, A., Piehler, J., Haase, W., Hahn, S., Dötsch, V., and Bernhard, F. (2007) Cell-free production of G protein-coupled receptors for functional and structural studies. *J. Struct. Biol. 158*, 482–493.
42. Kalmbach, R., Chizhov, I., Schumacher, M. C., Friedrich, T., Bamberg, E., and Engelhard, M. (2007) Functional cell-free synthesis of a seven helix membrane protein: In situ insertion of bacteriorhodopsin into liposomes. *J. Mol. Biol. 371*, 639–648.
43. Schwarz, D., Klammt, C., Koglin, A., Löhr, F., Schneider, B., Dötsch, V., and Bernhard, F. (2007) Preparative scale cell-free expression systems: New tools for the large scale preparation of integral membrane proteins for functional and structural studies. *Methods 41*, 355–369.
44. Sukharev, S. I., Blount, P., Martinac, B., Blattner, F. R., and Kung, C. (1994) A large-conductance mechanosensitive channel in *E. coli* encoded by mscL alone. *Nature 368*, 265–268.
45. Busch, A. E., Quester, S., Ulzheimer, J. C., Waldegger, S., Gorboulev, V., Arndt, P., Lang, F., and Koepsell, H. (1996) Electrogenic properties and substrate specificity of the polyspecific rat cation transporter rOCT1. *J. Biol. Chem. 271*, 32599–32604.
46. Koepsell, H., Korn, K., Ferguson, D., Menuhr, H., Ollig, D., and Haase, W. (1984) Reconstitution and partial purification of several Na^+ cotransport systems from renal brush-border membranes. Properties of the L-glutamate transporter in proteoliposomes. *J. Biol. Chem. 259*, 6548–6558.
47. Ducis, I., and Koepsell, H. (1983) A simple liposomal system to reconstitute and assay highly efficient Na^+/D-glucose cotransport from kidney brush-border membranes. *Biochim. Biophys. Acta 730*, 119–129.
48. Shimada, H., Moewes, B., and Burckhardt, G. (1987) Indirect coupling to Na^+ of p-aminohippurate uptake into rat renal basolateral membrane vesicles. *Am. J. Physiol. 253*, F795–F801.
49. Pritchard, J. B. (1988) Coupled transport of p-aminohippurate by rat kidney basolateral membrane vesicles. *Am. J. Physiol. 255*, F597–F604.
50. Aslamkhan, A., Han, Y.-H., Walden, R., Sweet, D. H., and Pritchard, J. B. (2003) Stoichiometry of organic anion/dicarboxylate exchange in membrane vesicles from rat renal cortex and hOAT1-expressing cells. *Am. J. Physiol. 285*, F775–F783.
51. Schmitt, C., and Burckhardt, G. (1993) p-Aminohippurate/2-oxoglutarate exchange in bovine renal brush-border and basolateral membrane vesicles. *Pfluegers Arch. 423*, 280–290.
52. Inui, K., Takano, M., Okano, T., and Hori, R. (1986) Role of chloride on carrier-mediated transport of p-aminohippurate in rat renal basolateral membrane vesicles. *Biochim. Biophys. Acta 855*, 425–428.
53. Schmitt, C., and Burckhardt, G. (1993) Modulation by anions of p-aminohippurate transport in bovine renal basolateral membrane vesicles. *Pfluegers Arch. 425*, 241–247.

BI800060W